JOURNAL OF PROPULSION AND POWER
Vol. 24, No. 5, September–October 2008

Hypersonic Flow Control Using Surface Plasma Actuator

J. S. Shang*
Wright State University, Dayton, Ohio 45435
R. L. Kimmel†
Air Force Research Laboratory, Wright–Patterson Air Force Base, Ohio 45435
J. Menart‡
Wright State University, Dayton, Ohio 45435
and
S. T. Surzhikov§
Russian Academy of Science, 119526, Moscow, Russia

DOI: 10.2514/1.24413

Plasma-fluid-dynamic interaction has been shown to be a viable mechanism for hypersonic flow control. An effective and verified flow control process using direct current surface discharge is summarized. The operating principle is based on a small electromagnetic perturbation to the growth rate of the displacement thickness of a shear layer that is strongly amplified by a subsequent pressure interaction. The aerodynamic control is delivered in less than a millisecond time frame and produces no parasitic effect when deactivated. The magnitude of the resultant aerodynamic force and moment can be significant and does not require a large amount of power for plasma generation to overcome the inefficient ionizing process, thus reducing the weight of a high-speed vehicle. The electromagnetic perturbation is derived from a surface gas discharge with or without an externally applied magnetic field. An embedded plasma actuator near the leading edge of a flat plate has produced high surface pressure equivalent to more than a 5 deg flow deflection at Mach 5, and the flow control effectiveness will increase with an increasing oncoming Mach number. The detailed flow structure of weakly ionized airstreams has been investigated by a combination of experimental effort and computational simulation solving the magneto-fluid-dynamic equations in the low magnetic Reynolds number limit with a drift-diffusion plasma model. The identical plasma actuator is investigated as a variable geometry cowl of a hypersonic inlet. All phenomena are replicated by computational results and are fully validated by experimental observations.

Nomenclature

$\mathbf{B}$	=	magnetic flux density
$\mathbf{D}$	=	electric displacement
$\mathbf{E}$	=	electric field strength
e	=	specific internal energy
$\mathbf{H}$	=	magnetic field strength
$\mathbf{J}$	=	electric current density
n	=	charged particle number density
Re_m	=	magnetic Reynolds number, $Re_m = \mu_m \sigma u L$
S	=	Stuart number $S = \sigma B^2 L/\rho u$
$\mathbf{u}$	=	velocity vector
ε	=	electrical permittivity
ρ	=	gas mixture density
ρ_e	=	charged particle density
σ	=	electrical conductivity
$\boldsymbol{\tau}$	=	molecular stress tensor
μ_m	=	magnetic permeability

Received 3 April 2006; revision received 25 March 2008; accepted for publication 25 March 2008.

*Research Professor, Emeritus Scientist. Fellow AIAA.
†Research Scientist. Associate Fellow AAIA.
‡Associate Professor. Member AIAA.
§Deputy Director and Professor of Institute for Problems in Mechanics. Associate Fellow AIAA.

Introduction

IMPRESSIVE progress has been made in a broad spectrum of plasma actuator research for flow control [1,2]. The gist of the idea is expanding the physical dimension of flow control mechanisms to include electromagnetic force and energy. The principle components are the Lorentz acceleration and Joule dissipation, and these electromagnetic phenomena can exist only in the electrically conducting fluid medium of a flowfield. This transport property is achievable by excitation of higher internal degrees of freedom of gas molecules via ionization. In most applications, the ionization processes are limited to thermal and electron collision [3,4]. In both processes, a substantial amount of energy is required to excite the molecules to elevate them from the stable ground to electronic state, and a significant portion of this energy is absorbed by the heat of formation and cascades into vibration excitation. Meanwhile, sustaining ionization must be maintained to offset the depletion of charged particles by recombination, attachment, dissipation, and diffusion. Therefore, the effectiveness of the flow control using plasma actuation is closely tied to the energy efficiency of the ionizing process.

For low-speed flow control, the alternating current dielectric barrier discharge (DBD) is the most widely used for plasma generation [5–8]. A periodic electrostatic force is generated by the applied electric field on separated charged particles immediately adjacent to the pair of exposed and encapsulated electrodes. The maximum intensity of the force per unit volume can be very high but is sustained only for a short duration in a kHz frequency range. According to Boeuf and Pitchford [9], the force per unit volume averaged in time is around 10^3 N/m^3 or one dyne/cm^3. This value agrees very well with an independent numerical simulation by Shang [10], who used Maxwell's equations to describe the electric field over a DBD and calculated the charged particle concentration by a drift-diffusion model. Even though this force is rather small in comparison with the inertia of most fluid motions, the momentum transfer in the

plasma sheath between ions and neutral particles creates a wall jet parallel to the electrodes. The magnitude of the velocity can attain a value over 4 m/s, and in the innermost region of a shear layer, it has been very effective for flow control [5,7]. Therefore, it is not surprising that all experimental evidence and numerical simulations show that this type of plasma actuator is most effective when applied at bifurcation points of the flowfield [8,11–13]. Successful applications are noted at the point of flow separation on the airfoil or near the dynamic stall of wings [8,10–13]. Numerical simulations using plasma models also indicate that the effectiveness of flow control is striking at the lower Reynolds numbers but diminishes rapidly in the high Reynolds number domain. This observation is easily understood because, under this flow condition, the inertia of fluid motion is dominant, and the thinning of the plasma sheath reduces the collision cross section for momentum transfer between ion and neutral particles [10,12].

Innovative and attractive ideas for a complete hypersonic propulsive system have been put forward, but further development has been inhibited by a limited ability to analyze the extremely complex physics, and the assessment of these revolutionary concepts remains inconclusive [14–16]. However, it is still logical to seek improvement to aerodynamic performance through magneto-fluid-dynamic (MFD) interaction because the weakly ionized gas is frequently encountered in hypersonic flow [17,18]. The ionization fraction is relatively low, and even at reentry conditions, the electrical conductivity is limited to a value around 100 mho/m [19]. Therefore, the concentration of charged particles must be enriched for an effective MFD interaction. A few years ago, the energy deposition by injection through a counterflowing plasma jet from the stagnation point of a blunt body for drag reduction was advocated by Ganiev et al. [20]. Indeed the wave drag reduction for a hypersonic blunt body flow has exceeded more than 50%; however, the major contribution to the reduced drag is derived from the counterflowing jet and bow shock interaction. In a series of side-by-side computational and experimental investigations by Shang et al. [21,22], the major portion of the wave drag reduction was found to be derived from a single bow shock degeneration into a multiple shock structure. The system of shocks over a counterflowing jet consists of a Mach disk that terminates the plasma jet, a ring shock, and a much weakened bow shock.

The mechanism of remote energy deposition has since become more sophisticated; the energy is introduced into the flowfield through either a broadband microwave or laser beam [23–27]. For laser energy deposition, the initial energy release to electrons by multiphoton ionization leads to a rapid expansion of plasma appearing as a detonation wave. The electrons also absorb the laser radiation as a result of electron-neutral inverse bremsstrahlung collisions [24]. The energy is released at a predetermined location upstream to a hypersonic vehicle. The suddenly released energy triggers a blast wave that modifies the thermodynamic properties of the oncoming stream through a lower Mach number and complex shock-on-shock interaction. The pulsating chemical kinetics and fluid dynamic interactions are very complex and must be accurately analyzed to fully understand the phenomenon of plasma discharge in space [23,24,27].

Most recently, hypersonic flow control using surface discharge has shown promise to achieve the desired effectiveness [28–36]. One of the reasons is that the power supply and implementation of surface plasma is much less elaborate, and the ionizing process is more efficient than space discharge. In general, an enormous amount of energy is needed to generate volumetric plasma that must have a sufficient charged particle number density for strong MFD interaction [28,29]. Even if the simple electronic collision process is employed for plasma generation, the ionization potential always underestimates the energy requirement, because the nonequilibrium energy cascades to vibration excitation and losses to diffusion, recombination, and attachment processes [3]. In magnetohydrodynamic applications, the strong magneto-fluid-dynamic interaction was further enhanced by an externally applied magnetic field [21]. The relative magnitude of electromagnetic force to the fluid inertia is described by an interaction parameter, the Stuart number $S = \sigma B^2 L/\rho u$ [37]. The presence of a magnetic field introduces additional complications in the forms of the Hall current and ion slip for the partially ionized gas, but the magneto-fluid-dynamic interaction is accentuated when the magnetic field intensity is high and the fluid inertia is low [37,38]. Magnetic field intensity is maximal at the magnetic poles, and the fluid inertia is minimal near solid surfaces. Therefore, the most effective placement of plasma actuators is obvious.

Another key reason using surface plasma discharge for hypersonic flow control is to take advantage of an intrinsic characteristic of high-speed flows. The strong viscous–inviscid interaction is a unique feature of hypersonic flow, in that the presence a boundary layer is no longer negligible. The displacement thickness produces an outward flow deflection, leading to compression waves and coalescing into a shock wave. The induced shock wave in turn modifies the boundary-layer structure to close the interacting loop. The classic hypersonic flow theory by Hayes and Probstein describes the inviscid–viscous interaction over a sharp leading edge as the pressure interaction [39]. The pressure distribution near the leading edge of a solid surface can be substantially altered by an electromagnetic perturbation to the growth rate of the displacement thickness of the boundary layer. Through the tangent wedge or tangent cone approximation, the magnitude of the induced pressure can be calculated by a single interaction parameter $\chi = M^3(C/Re)^{1/2}$. The viscous–inviscid interaction is strongly accentuated in hypersonic flows by the oncoming Mach number. Several experimental and computational investigations have focused on exploiting this characteristic by introducing electromagnetic perturbation for flow control [29–35]. This control mechanism can be actuated in milliseconds to deflect the flow from a solid surface, emulating a movable leading edge strake and equally applicable as the variable geometric cowl of a hypersonic inlet [35]. Preliminary results from both experimental and computational efforts have shown promise that the chain of events, including the MFD and inviscid–viscous interactions, constitutes a very effective hypersonic flow control technique with a simple surface discharge.

High-speed flow control using surface discharge has been investigated for some time. In fact, Leonov et al. [36] has applied pulsed direct current discharge (DCD) for flow control in subsonic, transonic, and supersonic flows. The surface discharge affects the flowfield through the Joule and electrode heating, electrostatic force, and electromagnetic force, with or without an externally applied magnetic field. These phenomena are best investigated by a combination of experimental and computational efforts [29–35]. Menart et al. [31,32] and Kimmel et al. [33] have observed that a dc surface charge produced a local surface pressure rise over the embedded electrodes on a flat plate at Mach 5. Their observations were made even without an imposed magnetic field. An imposed magnetic field normal to the electrode surface substantially modifies the induced surface pressure through the ionization process and produces a Lorentz force in the discharge domain. The basic MFD interacting phenomenon has been anticipated in designing these experiments [29]. Meanwhile, integrated experimental and numerical simulations by Shang et al. [29,30] have firmly demonstrated the unique hypersonic flow control achieved through a combination of electromagnetic perturbation and inviscid–viscous interaction. Now, flow control using MFD interaction has been successfully implemented within a constant, cross-sectional, rectangular hypersonic inlet to mimic a variable geometry cowl [35].

During these investigations, it was found that the most challenging issue of both experimental and computational efforts for MFD interaction resides in the description of transport properties of the plasma. In most laboratory experiments, weakly ionized gas is generated by electron collision with embedded electrodes on control surfaces [5–8,17,18,31–36]. This mechanism is also most likely to be used for enriching the charged particle number density in practical applications. The generated plasma consists of electrons in a highly excited state, but the heavy ions retain the thermodynamic condition of the surrounding neutral particles [3,4]. Most important of all, the surface plasma generated by electronic collision is far from thermodynamic equilibrium. For flow control using electromagnetic

forces, the degree of ionization, electrical conductivity, current density, and electrical field strength of the plasma are critical. To generate a physics-based computational simulation for better understanding and to quantify results that cannot be obtained from experimental observations alone, a group of plasma models built on drift-diffusion theory including an externally applied magnetic field have been developed by Surzhikov et al. [40,41]. Therefore, physics for these plasma models must be validated by comparison with available data before application.

In the present effort, the pertinent characteristics of surface discharges for MFD interaction are studied by comparing with available data in a hypersonic plasma channel [42]. Then, the results of MFD interaction over the leading edge of a control surface, with and without an externally applied magnetic field, are presented to distinguish the effects of Lorentz force and Joule heating. Finally, the MFD compression activated in the entrance region of a rectangular, constant, cross-sectional inlet to emulate a variable geometric cowl is also demonstrated and delineated.

Governing Equations

The governing equations of magnetoaerodynamics are the combination of the time-dependent compressible Navier–Stokes and the Maxwell equations in the time domain [37,38]. From the intrinsic characteristics of plasma, the displacement electrical current, $\partial \mathbf{D}/\partial t$, has a negligible value in comparison to the conducting current, $\sigma \mathbf{E}$. In an electric field with a radian frequency ϖ the ratio of $(\partial \mathbf{D}/\partial t)/(\sigma \mathbf{E})$ is $\varepsilon \varpi/\sigma$ or $10^{-13}\varpi$. According to Sutton et al. [37], the displacement current can be neglected even at microwave frequency. Similarly, in an airstream that flows at a velocity of 10^5 m/s with a linear varying electrical field, the ratio of the transport of excess charges to the conducting electric current $(\rho_e \mathbf{u})/(\sigma \mathbf{E})$ has a value of 10^{-8}. Therefore, in a plasma field, the generalized Ampere's law and Gauss's law for electric displacement can be further simplified by the intrinsic plasma properties. The combined Navier–Stokes and simplified Maxwell equations for magnetoaerodynamics become [37]

$$\partial \rho/\partial t + \nabla \cdot (\rho \mathbf{u}) = 0 \tag{1}$$

$$\partial \mathbf{B}/\partial t + \nabla \cdot (\mathbf{uB} - \mathbf{Bu}) = -\nabla \cdot [(\nabla \cdot \mathbf{B}/\mu_m)/\sigma] \tag{2}$$

$$\partial \rho \mathbf{u}/\partial t + \nabla \cdot [\rho \mathbf{uu} - \mathbf{BB}/\mu_m + (p + B^2/2\mu_m)\mathbf{I} - \boldsymbol{\tau}] = 0 \tag{3}$$

$$\partial \rho e/\partial t + \nabla \cdot [(\rho e + p)\mathbf{u} + \mathbf{q} - \mathbf{u} \cdot \boldsymbol{\tau}] = (\nabla \cdot \mathbf{B}/\mu_m)2 \tag{4}$$

where $\mathbf{uu}$ and $\mathbf{BB}$ are the dyadics of the velocity and magnetic flux density. In these formulation, the dominant electromagnetic wave motion is strongly emphasized. From the eigenvalue analysis of the ideal magnetohydrodynamic equation, four distinct wave components are easily identified in the plasma medium. They are the longitudinal sonic wave, transverse Alfven wave, and fast and slow magnetoacoustic waves [43].

For most aerospace applications, the magnetic Reynolds number $Re_m = uL/(\mu_m \sigma)^{-1}$ is much less than unity ($Re_m \ll 1$), which means the induced magnetic flux density $\mathbf{B}$ is negligible in comparison with the externally applied field [37,38]. Under this circumstance, Faraday's induction law of the Maxwell equations can be decoupled from the rest. This approximation now shifts emphasis from the study of electromagnetic wave motion to magneto-aerodynamic force interaction. In this formulation, the Lorentz force and Joule heating appear as source terms in the modified Navier–Stokes equations. In general, the electrostatic force $\rho_e \mathbf{E}$ is negligible, and the ratio of magnitude of Lorentz force and electrostatic force is in the order of 10^{-8} [37]. The resultant governing equations and the initial values and boundary conditions are substantially simplified. A very large group of numerical simulations have demonstrated the ability of these governing equations to accurately predict a wide range of magnetoaerodynamic interactions [11–13,16,29,30,35,40,41]:

$$\partial \rho/\partial t + \nabla \cdot (\rho \mathbf{u}) = 0 \tag{5}$$

$$\partial \rho \mathbf{u}/\partial t + \nabla \cdot (\rho \mathbf{uu} + p\mathbf{I} - \boldsymbol{\tau}) = \mathbf{J} \cdot \mathbf{B} \tag{6}$$

$$\partial \rho e/\partial t + \nabla \cdot [(\rho e + p)\mathbf{u} - \mathbf{q} - \mathbf{u} \cdot \boldsymbol{\tau}] = \mathbf{E} \cdot \mathbf{J} \tag{7}$$

To ensure consistent electrical field intensity for the low magnetic Reynolds number approximation, the charge conservation equation is included into the system of governing equations. This equation satisfies both Ampere's circuit law and Gauss's law for electrical fields

$$\partial \rho_e/\partial t + \nabla \cdot \mathbf{J} = 0 \tag{8}$$

An alternative approach using Eq. (8) is to explicitly satisfy Gauss's law for electrical fields:

$$\nabla \cdot (\varepsilon E) = \rho_e \tag{9}$$

In the steady-state asymptote, Faraday's induction law indicates that the curl of $\mathbf{E}$ vanishes, and the electric field intensity can be defined by an electric potential $\mathbf{E} = -\nabla \varphi$. Both Eqs. (8) and (9) reduce into the Poisson equation for the electrical potential [40].

Because the basic partial differential system consists mainly of the compressible Navier–Stokes equations, all traditional flux-splitting formulations and solving procedures are directly usable. Accordingly, the system of equations can be cast easily into the flux vector form and solved by numerical procedures developed in the computational fluid dynamics (CFD) community [11–13]. The boundary conditions for the aerodynamic variables are straightforward; the no-slip condition is imposed for all velocity components, a constant wall temperature or adiabatic wall condition describes the condition on solid surfaces, and the vanishing pressure gradient condition provides the value of density locally. At the far field, the flow returns to its unperturbed state beyond the shock envelope. In hypersonic flow, the traditional no-change condition applies at the downstream far field. For the electromagnetic variable, in general, the tangential component of the electrical field intensity and the normal component of the magnetic flux density are continuous across media interfaces.

Plasma Models

The long-range Coulomb force dominates the collective behavior of charged particles [38]. This observation is independent of how the gas discharge is generated. Ionization by electron collision is widely used for flow control; however, the physical understanding of this phenomenon is still limited. A part of the reason is that the physical phenomenon is very complex and involves interaction at the atomic level. Nevertheless, an electric field of sufficient intensity generates electron-ion pairs by electron impact ionization of the neutral gas. The avalanche produced by secondary emission from the electrodes is also a source of the electron generation process. In the discharge region between electrodes, the current consists of conduction and displacement electrical current components. In a dc field, only the conductive current flows, and it is the consequence of the relative motions of electrons and positively charged ions. In an AC field, the displacement current increases with frequency whereas the importance of secondary emission diminishes [3,4].

The drift-diffusion and a quasi-neutral plasma models by Surzhikov and Shang [40,41] have been successfully developed for dc discharge in a magnetic field. It is well known that the drift-diffusion plasma model is inadequate in describing the sheath regions of the electrodes [3]. However, the model is still able to predict all general features of the glow discharge with sufficient accuracy for applied physics and engineering applications [9–12,29,30]. This group of models contains both multifluid and multitemperature formulation for all charged particles including electrons and positive and negative charged ions. An practical plasma description is probably the quasi neutral or the ambipolar model, which has

performed adequately up to moderate pressures $p > 50$ torr [29,30]. However, accurate simulations are severely limited to an extremely high-altitude environment in which the pressure is only a few torr. To apply plasma flow control to practical applications, the limitation of plasma generation to low-pressure or low-density conditions must be alleviated. There are numerous surface plasma generation processes that can reliably function in a high-pressure environment to augment the low electrical conductivity in a weakly ionized gas [3–5,17,27].

From a phenomenological viewpoint, the principal mechanisms of the motion of charged particles are the drift velocity and diffusion; in addition, the different diffusion velocities between electrons and ions restrain electron movement [3,4]. This component of diffusion is referred to as ambipolar diffusion. Again, in a self-sustained plasma, the rate of change for charged number density in a control volume is mainly balanced by generation through ionization and depletion by recombination. The continuity equations for species concentration of the two-component plasma are given by the drift-diffusion theory [40,41]:

$$\partial n_e/\partial t + \nabla \cdot \Gamma_e = \alpha(E, p)|\Gamma_e| - \beta n_+ n_e \tag{10}$$

$$\partial n_+/\partial t + \nabla \cdot \Gamma_+ = \alpha(E, p)|\Gamma_e| - \beta n_+ n_e \tag{11}$$

where $\Gamma_e = -D_e \nabla n_e - n_e \mu_e \mathbf{E}$ and $\Gamma_+ = -D_+ \nabla n_+ + n_+ \mu_+ \mathbf{E}$ are the electron and ion flux densities, respectively. In this formulation, $\alpha(E, p)$ and β are the first Townsend ionization coefficient and recombination coefficient, μ_e and μ_+ are the electron and ion mobility, and D_e and D_+ are the electron and ion diffusion coefficients [3,4]. The electrical current density, by definition, is given by $\mathbf{J} = e(\Gamma_+ - \Gamma_e)$.

In most electrodynamic formulations, the electrical field intensity is replaced by an electrical potential function $\mathbf{E} = -\nabla\varphi$. The compatibility condition, either Eq. (8) and (9), leads to the well-known Poisson equation for the electrical potential φ [37,38]:

$$\nabla^2 \varphi = 4\pi e(n_e - n_+) \tag{12}$$

In the presence of an externally applied magnetic field that has only a transverse component B_z, the modification to the electrodynamic equation is straightforward. The effect of the magnetic field can be easily accommodated by introducing an effective electrical field as in [37,38]. Through this formulation, the Hall effect can be included by explicitly modifying the mobility, diffusion of ions and electrons, and ionization coefficients of the drift-diffusion theory. These modifications are equally applicable to the ambipolar model [40,41]:

$$\mu_e = \mu_e/(1 + b_e^2) \tag{13a}$$

$$\mu_e^* \approx (\mu_e + \mu_+)/[(1 + b_e^2)\mu_+ + \mu_e] \tag{13b}$$

$$D_e = D_e/(1 + b_e^2) \tag{13c}$$

$$D_a = (\mu_+ D_e + \mu_e D_+)/(\mu_e + \mu_+) \tag{13d}$$

$$\alpha(E, p) = \alpha(E, p)/(1 + b_e^2) \tag{13e}$$

where $b_e = \varpi_e/m_e C$ and $b_+ = \varpi_+/m_e C$ are the Hall parameter for the electron and ion, and ϖ_e and ϖ_+ are the Cyclotron or Larmor frequency of the electron and ion, respectively [38]. C is the speed of light.

A quasi-neutral model of direct current discharge in a magnetic field can also be formulated by using the intrinsic property of plasma as a simplified approximation [40,41]. The conservation equation for the charged particles becomes

$$\partial n/\partial t + \nabla \cdot (\mathbf{u} n - \mu_e^* D_a \nabla n) = \omega_e \tag{14}$$

This model is frequently referred to as the ambipolar model [41]. The source term in the species conservation equation in a magnetic field is modified to appear as

$$\omega_e = (\alpha/p^*)p^* E \mu_e(p^*)/(1 + b_e^2) - \beta n^2 \tag{15}$$

The electrical field intensity E in the low magnetic Reynolds number limit must satisfy the charge conservation equation and the global neutral condition to be compatible with the drift-diffusion formulation. For the simpler phenomenological model, the compatibility condition also requires invocation of the generalized Ohm's law:

$$\nabla \cdot [(\mu_+ + \mu_e^*)nE + (D_e^* - D_+)\nabla n] = 0 \tag{16}$$

For the drift-diffusion models, the appropriate boundary condition on the cathode requires enforcement of zero electrical potential, and the number density of electrons is proportional to the coefficient of secondary electron emission [40,41]. It is assumed that the anode reflects all ions; the number density of the ion vanishes, and electrical potential is prescribed by the difference over the electrodes. On the dielectric surface, the charged number density is negligible, and the outward normal gradient of the electrical potential is zero.

Features of Direct Current Discharges

For ionizations by electronic collisions, the basic direct current discharge structure is sustained by an electric field. The simplest electrode placement is the parallel plate configuration in which the cathode and anode are separated by a small gap across an applied electrical field. Both computational and experimental investigations were performed to validate the drift-diffusion plasma model with and without a transversal magnetic field [40,41].

Figure 1 presents a computational stationary dc discharge using the drift-diffusion plasma model [40]. The numerical simulation is conducted for a glow discharge between parallel electrodes with a gap distance of 20 mm and at an ambient pressure of 5 torr. This surface discharge is maintained by an applied electric field of 1.2 kV, and the maximum current density on the anode is 6.0 mA/cm^2. The computational simulation captures all essential features of a dc discharge that have been established by classic investigations [3,4]. In the cathode fall of the electric potential in the cathode layer, the charge separation in the plasma sheath regions and the nearly linear electric field beyond the cathode layer and over most of the discharge column are clearly displayed. Computed results also show that deceasing the ambient pressure leads to a considerable increase not only in the width of the discharge, but also the thickness of the cathode layer. These numerical simulations are in a good agreement with classic theory [40].

The Lorentz force exerts a strong influence on the dc discharge structure when an external magnetic field is applied. This behavior is

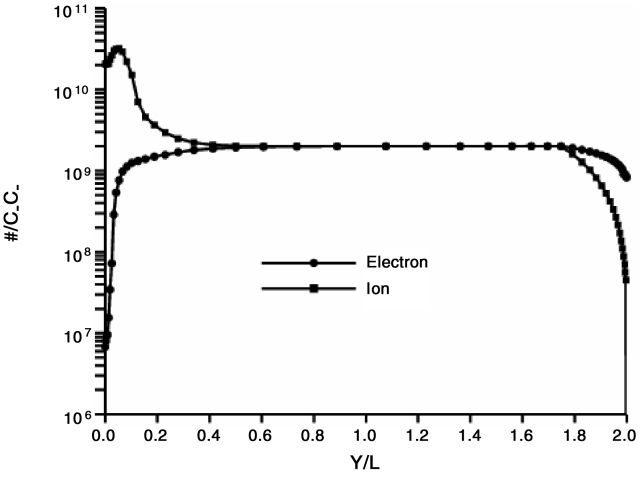

Fig. 1 Glow discharge between parallel electrodes EMF = 800 V (electromotive force), $P = 5.0$ torr, $L = 20$ mm.

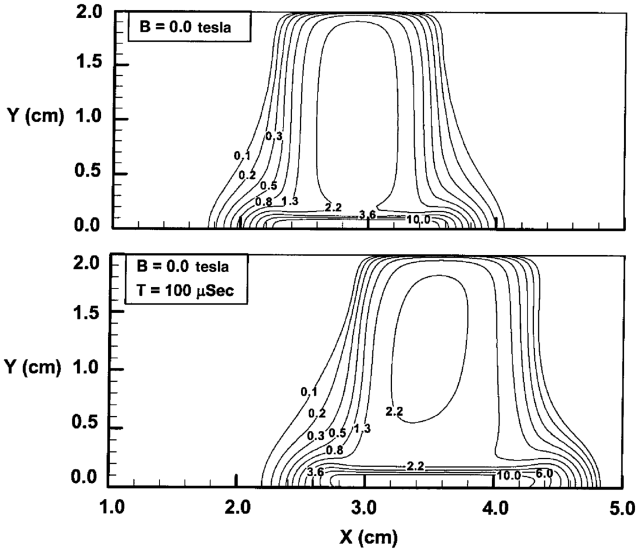

Fig. 2 Ion number density contours of dc discharge (in $10^9/cm^3$) with transverse external magnetic field EMF = 2.0 kV, $P = 5.0$ torr, $L = 20$ mm, $B = 0.01$ T.

easily detected from the computational simulations in Fig. 2. The dc discharges were sustained by an electrical potential of 2.0 kV and at an ambient pressure of 5.0 torr with a gap of 20 mm between electrodes. The ion number density distribution in the absence of a magnetic field is stationary and has a maximum value of $10^{10}/cm^3$ immediately over the cathode. As soon as a transverse magnetic field is applied, the discharge column is moved continuously along electrode surfaces even by a relatively weak external field as low as 0.01 T. Because of the nature of ambipolar diffusion, the shift velocity is much less than electronic drift velocities but is greater than the ionic drift velocities. The shift velocity is perpendicular to the applied magnetic field and proportional to the strength of the field. The computed velocity varies from 6.5×10^2 to 3.5×10^3 m/s with respect to a magnetic intensity of 0.01 and 0.05 T [40]. The direction of the shift velocity of the discharge column is dictated by the polarity of the applied magnetic field; by reversing the transverse magnetic field polarity, the discharge column moves in the opposite direction.

The first validation of numerical simulations is achieved by a direct comparison of ion number density profiles over a side-by-side electrode arrangement. This configuration is the basic embedded electrodes arrangement for hypersonic flow control to prevent any unintended intrusion into the flowfield. The cathode is placed upstream of the anode and close to the leading edge of a control surface. For the present study, the electrodes have a separation distance of 38.1 mm. To support practical applications, the comparison of computation and data are conducted in a Mach number 5.15 hypersonic plasma channel [31,32]. The stream has a velocity of 675.5 m/s and the static pressure and temperature of 0.6 torr (78.4 Pa) and 43 k. The dc discharge was ignited by an electric potential of 1.2 kV; under this condition, the mass fraction of charged particles less than 10^{-5}. In Fig. 3, the computed ion number density profile over the anode attains an excellent agreement with data measured by a double Langmuir probe with a sensing area of 5.03×10^{-4} mm^2. The ion number density profile over the cathode shows a discrepancy compared with the data, but the difference is confined within the data scattering band between measurements using the Langmuir probing and microwave absorption technique [31,42].

Another major phenomenon that appears in MFD interaction is Joule heating. It is the consequence of an electrical current moving through a lossy medium like plasma. The electrical energy is dissipated from the component of the current perpendicular to the magnetic induction field; therefore it is not affected by the Hall parameter but by ion slip [36]. Joule heating is often viewed as a detrimental effect in plasma physics, but becomes an effective volumetric heating source in MFD interaction. The exact portion of

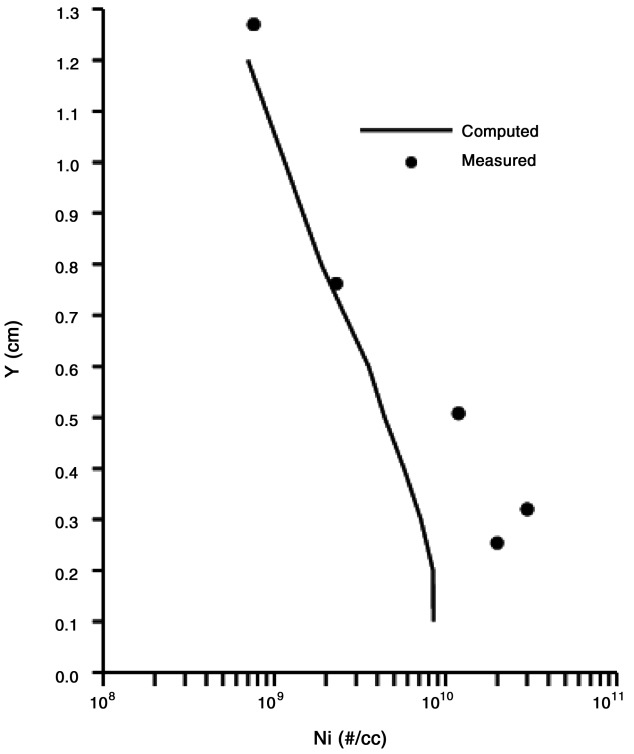

Fig. 3 Comparison of ion number density profiles over anode $P = 0.6$ torr, EMF = 800 V, $I = 50$ mA, $L = 60$ mm.

energy dissipated by Joule heating for plasma generation is not known and depends on the quantum chemical physics process. However, the dissipated energy is anticipated to be just a small fraction after cascading into vibration–translation, vibration–vibration relaxations, and secondary chemical kinetics [28,40]. The computed Joule heating in a typical dc discharge from the side-by-side embedded electrodes configuration is depicted in Fig. 4. The computing simulation duplicates the experimental condition of the discharge in the hypersonic stream ($M_\infty = 5.15$) maintained by an electrical potential of 800 V and a total current of 50 mA in the electrical circuit. The Joule heating spans a range from 2.51×10^6 to 3.76×10^8 erg/cm^3; the maximum value is located above the outer edges of electrodes and within the plasma sheath over the solid surface.

Because a direct measurement of Joule heating is not achievable as a volumetric heat source, the verification can only be obtained by comparing the stagnation temperature profiles above the electrodes in Fig. 5. To duplicate the experimental condition, the computational simulation was conducted by assigning surface temperatures on the dielectric and electrode surface to be 300 and 560 K, respectively, according to the experimental observation. The data were collected by a total temperature probe [31–34,42]. In general, the computational simulation has achieved a reasonable agreement

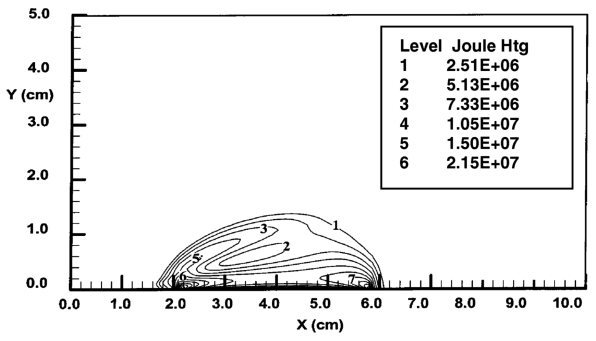

Fig. 4 Joule heating distribution of dc discharge (erg/cm^3) EMF = 800 V, $P = 0.6$ torr, $M_\infty = 5.15$.

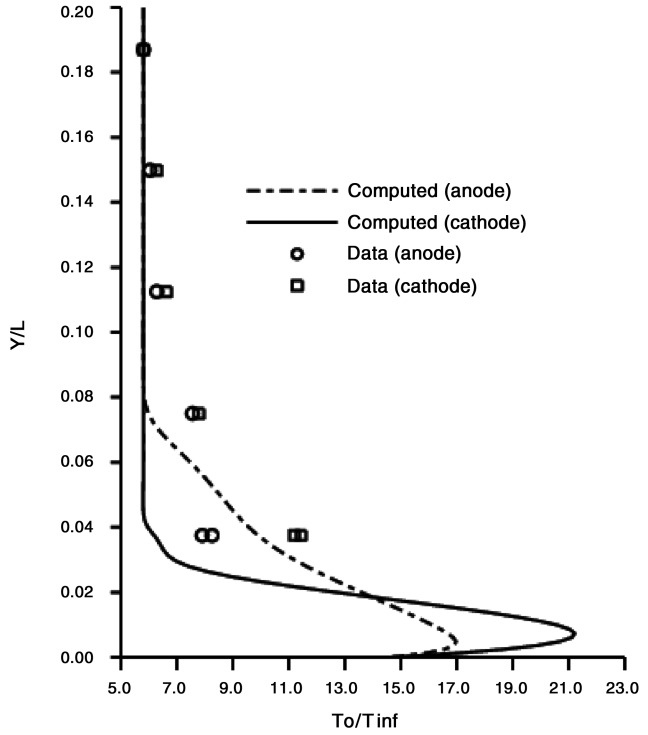

Fig. 5 Compare computed and measured stagnation temperature profiles, $M_\infty = 5.15$, $P = 0.6$ torr, $T_w = 300$ k, $T_{\text{electrodes}} = 560$ k.

with the data. Both results indicate that the Joule heating is more intense in the cathode than the anode layer. The volumetric heating in the inner region of the boundary layer also becomes obvious by showing the heat actually transfers from the gas stream into the electrode surface. Although the detailed near surface measurement is unobtainable due to the finite size of the probe, the direct comparison has provided a reasonable assurance that the drift-diffusion plasma model can capture the essential physics of the dc discharge for MFD interactions.

Inviscid–Viscous Interaction

A unique feature of hypersonic flow is the strong viscous–inviscid interaction, and two major types of interaction are well known [39]. The first type is the pressure interaction near a sharp leading edge involving the Mach waves, flow deflection angle, and the surface pressure. The other type is known as the vorticity interaction, which involves the boundary-layer structure and the vorticity of the external flow even if the layer is relatively thin. The vorticity interaction is always associated with blunt body flows, and the effect is more pronounced in the surface shear than heat transfer. For flow control using plasma actuators, the most effective mechanism is the pressure interaction in the leading edge domain of a control surface.

In hypersonic flow, the relatively small outward streamline displacement resulting from the presence of a boundary layer is no longer negligible. The streamline deflection is amplified by the square value of the freestream Mach number at low supersonic speed [39]. On a slender body or a sharp leading edge, the local streamline deflection induced by the boundary layer is of the reciprocal order of the square root of the Reynolds number, based on the running length from the leading edge. The product of the Mach number M and the flow local deflection angle Θ defines the hypersonic similitude parameter $M\Theta$. On a solid surface, the flow deflection angle is the sum of the local surface inclination Δ and the growth rate of the displacement thickness of a boundary layer $\Theta = \Delta + \partial\delta^*/\partial x$. Through a tangent cone or a tangent-wedge approximation, the induced surface pressure can be calculated accurately by a single pressure parameter $\chi = M^3(C/Rey)^{1/2}$. The pressure interaction is further classified into strong and weak interaction. For the weak pressure interaction $\chi < 3$, the displacement thickness of the

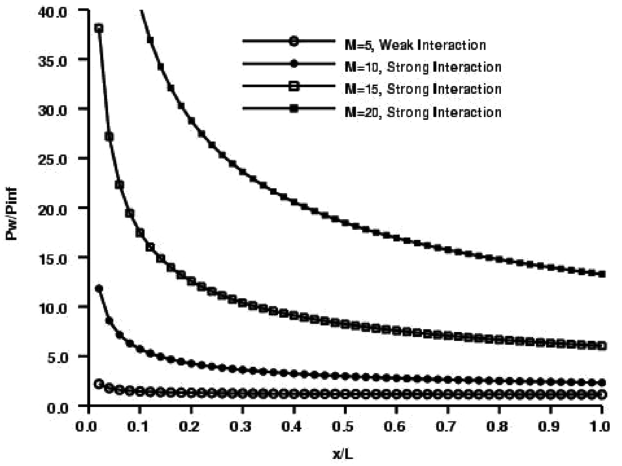

Fig. 6 Theoretic surface pressure generated by hypersonic pressure interaction at altitude of 50,000 m.

boundary layer remains unaltered. For the strong interaction, when the value of χ exceeds three, the boundary layer is affected by the interaction and grows according to a scale of $x^{3/4}$. In any event, the pressure interaction induces compression waves that coalesce into an oblique shock over the surface. This induced high-pressure region near the leading edge is the most favorable for generating a pitching moment for the control surface.

The pressure distributions over a sharp leading edge plate spanning a Mach number range from 5 to 20 are presented in Fig. 6. The numerical results are generated at an altitude of 50,000 m. Only a weak interaction can occur at the lower Mach number of 5. Beyond this Mach number, the phenomenon becomes a strong interaction. In fact, the value of χ increases to 3.41, 10.28, and 24.38 as the Mach number elevates to 10, 15, and 20. At the same Reynolds number, the surface pressure rise downstream of the leading edge steadily increases from 1.13, 2.51, 6.05, and 13.29, according to the Mach number from 5, 10, 15, to 20. In short, any small perturbation to the displacement thickness of a boundary layer in hypersonic flow can be strongly amplified by the intrinsic viscous–inviscid interaction. This mechanism can produce a significant control force and moment by a miniscule electromagnetic perturbation and is the operating principle of the studied plasma actuator for hypersonic flow control [29,30].

An electromagnetic perturbation to the inner shear layer can easily alter the growth rate of the boundary layer over the surface. The electromagnetic field with and without an external applied magnetic field can easily modify the growth rate of the displacement thickness in two aspects: changing the kinematics field structure and initiating heat exchange in the wall region. In a surface dc discharge, the local plasma heating is also derived from two distinct sources. One of them is the Joule heating, which is a volumetric energy conversion through the dissipation of conducting current in the plasma and is frequently referred to as the Ohmic heating. The other source of heat release is convection by the heated electrodes. For a dc discharge, the electrodes frequently attain a surface temperature approaching 600 K [31,32].

A schlieren photograph is depicted in Fig. 7. This image was obtained by dividing the wind-on image of the discharge by the windoff image to remove imperfection in the window glass. This image is recorded at the freestream Mach number of 5.15, a density of 5×10^{-3} kg/m^3. The dc discharge is generated by an electric potential of 800 V and with a total electrical current of 50 mA [32–34]. The measured maximum electron number density of the plasma is 3×10^{12}/cm^3. Through the dc surface discharge, the electrode and Joule heating lowers the local density and increases the boundary-layer displacement thickness. In turn, the increased slope of the displacement thickness induces a coalescing oblique shock resulting in a greater surface pressure over the plate surface. This image captures the key mechanism of the MFD flow control device. In this chain of events, the energy requirement for plasma generation is extremely limited, but the induced pressure rise is sufficient for flow

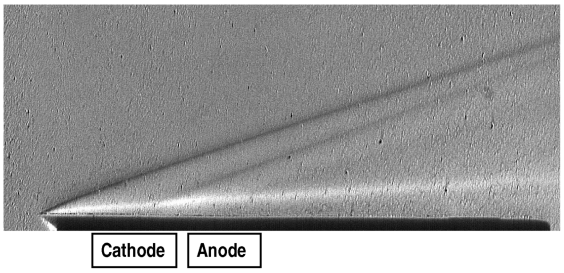

Fig. 7 Composite schlieren photographs of dc discharge over a plate surface $M = 5.15$, $V = 800$, $I = 50$ mA.

control. Furthermore the resultant surface pressure amplification is proportional to the freestream Mach number. In other words, if the electromagnetic perturbation can be sustained, the effectiveness for flow control is increased with a higher oncoming freestream Mach number.

The vastly different time scales between the convective electrode and volumetric Joule heating are illustrated in Fig. 8 from [30,31]. A Pitot probe was inserted into the flow downstream of the cathode. The discharge was turned on for periods of 5, 10, 20, and 40 s. It is seen that for the 40 s discharge, the Pitot pressure drops about 6% immediately after the discharge is turned off. After this, approximately 50 s is required for the pressure to decay to it undisturbed value. This slow decay indicates that electrode heating occurred during the discharge. As the plasma-on time decreases, the recovery time decreases. For the 5 s discharge, most of the Pitot-pressure decay occurs immediately after the plasma is turned off. In this case, the electrode and plate have had little time to heat during the discharge. The bulk of the observed effect is due to Joule heating. The Pitot pressure recovers quickly after the discharge is extinguished because the Joule heating ceases.

The magneto-fluid-dynamic interaction has also been applied for separation flow control [17,18,30]. In these applications, the electromagnetic force is introduced into a flow bifurcation not as a small perturbation but to energize the retarded shear flow to overcome an adverse pressure gradient. The MFD separated flow control derives from an active Lorentz force; thus, the control mechanism requires the presence of a strong externally applied transverse magnetic field. In principle, the separated flow control using electromagnetic forces can suppress the reversed flow over the solid surface and alleviate the degraded aerodynamic performance. However, there is a little realizable advantage to the viscous–inviscid interaction from amplifying the electromagnetic perturbation.

Virtual Control Surface

The electron-neutral collision frequency of a typical dc discharge in the present test facility is estimated to be between 10^6 and 10^8 Hz, and the collision cross section for momentum transfer is most likely between 10^{-17} and 10^{-16} cm^2 [42]. The ion-neutral collision frequency is much lower, and the collision cross section is greater than that of the electron-neutral collisions, but momentum transfer via collision between charged and neutral particles probably still would not be substantial. It is therefore not surprising to find that the electromagnetic force exerted by a dc discharge on the flowfield is negligible in comparison with the inertia of a hypersonic stream. The electrostatic force immediately adjacent to the electrodes is around 10^3 N/m^3 [9,10], and the Lorentz force of a dc discharge in the presence of a magnetic field of one tesla is about 50 N/m^3. However, the Joule heating can be significant, having a rate as high as 10^4 W/m^3 and mostly released in the plasma sheath [40].

A significant effect for hypersonic flow control using electromagnetic force, therefore, has to derive from the amplification of viscous–inviscid interaction. In fact, both experimental and computational investigations have shown the induced surface pressure near a sharp leading edge of a plate by hypersonic MFD interaction emulating a virtual pitching strake. This induced surface pressure on a fixed control surface behaves as if it had executed a pitching motion [32–34]. In all experiments, the plasma is generated between two electrodes embedded in the flat plate surface of a wedge model, and a total electrical current of 50 mA is maintained by an applied electric field of 1.2 kV in the circuit [32–34]. The maximum ion number density of the plasma is $3 \times 10^{12}/\text{cm}^3$, and the electrode temperature is estimated to be 600 K [31,32]. At a freestream static pressure of 0.59 torr and a static temperature of 43 K, the degree of ionization is 2.25×10^{-5}, and the electrical conductivity is on the order of 1 mho/m [31,42]. The gas discharge domain over the electrodes is merely a few cubic centimeters and is concentrated mostly over the electrode. In this sense, the dc discharge truly provides a surface layer of weakly ionized gas over the electrodes.

Experimental and computational investigations reveal that the volumetric Joule and convective electrode heating trigger additional compression waves above the electrodes through the thickening of the boundary-layer displacement thickness [29–34]. These waves coalesce and eventually merge with the oblique shock wave originating from the sharp leading edge. The resultant shock wave produces a high-pressure plateau over the wedge surface around the electrodes. This induced pressure plateau is a maximum near the leading edge of the electrodes and mimics a pitching movement of a leading edge strake. In Fig. 9, the relative magnitude of the conductive electrode and volumetric Joule heating is confirmed by experimental and computational results using plasma models [29,30,32]. The surface pressure plateau induced by the dc discharge is greater than that created by the electrode heating alone. In this regard, the dc discharge indeed generates a bona fide MFD interaction. At a very low power level of 60 W, the higher surface pressure ($p/p_\infty = 1.275$) from the MFD interaction is identical to a surface deflection of 1 deg at the freestream Mach number of 5.15. Experiments show that the power scaling for this interaction is

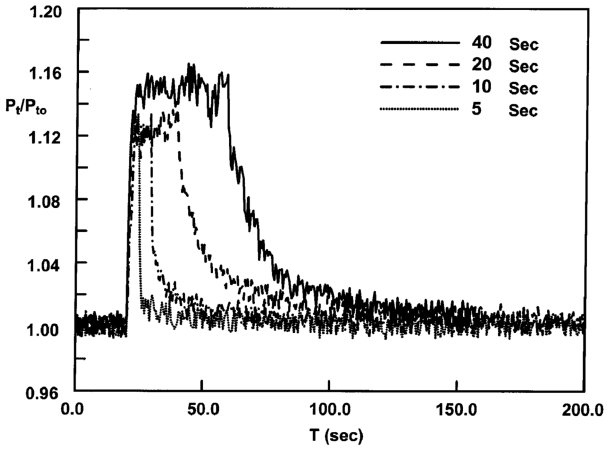

Fig. 8 Pitot-pressure response to ignited dc discharge of different durations $M_\infty = 5.15$, $Pt = 20.0$ torr, EMF = 1.2 kV, $I = 50$ mA.

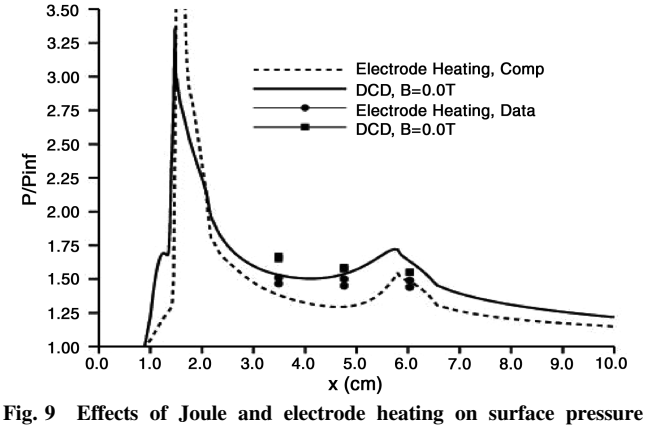

Fig. 9 Effects of Joule and electrode heating on surface pressure distributions $M_\infty = 5.15$, EMF = 1.2 kV, $I = 50$ mA, $P_0 = 370$ torr, $T_0 = 300$ k.

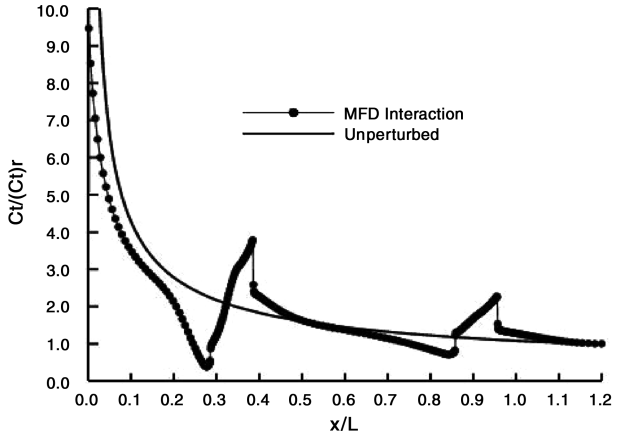

Fig. 10 Skin-friction coefficient distributions in dc discharge $M_\infty = 5.15, P_\infty = 0.59$ Torr, EMF = 1.2 kV, $I = 50$ mA.

18.90 W/cm per degree of equivalent deflection. At the maximum power input of 350 W for the dc discharge, the surface pressure distribution attains an equivalent streamline deflection over 7 deg [29,30]. However, the plasma generation process is now operated at the outer limit of an abnormal discharge mode.

In Fig. 10, the unique feature of viscous–inviscid interaction induced by the dc discharge becomes evident in the computed skin-friction distributions over the surface of the wedge model. For the purpose of comparison, the simulated skin-friction distributions are normalized by the far downstream asymptotes. When the dc discharge is absent, the distribution exhibits the classic behavior of a laminar boundary in a favorable pressure gradient near the sharp leading edge of the plate. In the presence of a dc discharge, the surface's shear reacts to the adverse and subsequently favorable pressure gradient upstream and downstream of the electrodes. The surface shear drops and rises responding to the local surface pressure behavior. However, the net change of the skin friction is nearly zero because the increased surface shear is nearly negated by the decreased upstream value. This observation is supported by experimental measurements [32,33,44]. Therefore, the virtual control surface by the MFD interaction generates mostly a lateral aerodynamic force but incurs negligible skin-friction drag.

The repeatable and rapid response performance for lift generation is further demonstrated in Fig. 11. The hypersonic MFD interaction is implemented on a small wedge model with a length and width dimension of 6.6 × 3.8 cm. The embedded cathode and anode stripe with a thickness of 0.06 cm have identical dimensions of 0.6 × 3.2 cm and are placed a distance of 2.9 cm apart. All data were collected at a Mach number of 5.15, stagnation pressure of 370 torr, and stagnation temperature of 270 K. The maximum data sampling rate of the experimental facility is one million points per second. During a 10-s test period, the plasma actuator is powered by a 3 Hz square wave current of 24 mA. The lift is measured by load cells and a laser displacement sensor [44]. Because the electrodes are placed on the upper surface of the small wedge model, the generated lift is negative and the total force is very limited. The magnitude of the mean lift increases over the first 4 s of the discharge, after which it is constant at −0.84 g. This long-time-scale trend is due to heating of the cathode and plate. This transient behavior is also observed in still air at an ambient pressure of 7 torr with zero lift. At shorter time scales, the generated lift follows the power input, and the rapid responses have the same peak-to-peak value for the entire testing period.

The full impact of MFD interaction requires the presence of an externally applied magnetic field [12–18,23–34]. A magnetic field exerts a profound effect on the plasma and alters characteristics of the plasma structure, including electrode sheaths [3,4]. Following the effective electric field formulation to account for the Hall current [37,38,40], the presence of a magnetic field is seen to affect the plasma generation via electron collisions. The basic phenomenon is governed by the reduced electron mobility in the magnetic field for plasma generation. In a dc discharge across parallel plates, the discharge column drifts in the direction associated with the polarity of a transverse magnetic field [40]. For a dc discharge in hypersonic flow control using electrodes of finite dimension, very little is known about the electrodynamic structure. One can only analyze it from the fundamental collision process and try to gain a better understanding from experimental observations [32–34].

In recent computing simulations of a dc discharge subjected to a transverse magnetic field, the magnetic field not only produces a substantial distortion of the discharge pattern but also induces a shift of the discharge column [40]. In plasma actuator applications of thin strip electrodes parallel to the leading edge, a similar behavior is also noted. Once a transverse magnetic field is applied across the plasma field, a movement of the high intensity attachment on the anode appears. The attachment changes its position based on the polarity of the magnetic field, and the most drastic phenomenon is the discharge constriction [32–34]. Figure 12 describes the applied voltage for plasma generation at a constant circuit current (50 mA) versus the transverse magnetic field. A large data scatter is noted in the measurements with and without an externally applied magnetic field. The voltage required to maintain the discharge drops with increasing magnetic field, up to a magnitude of about 0.3 T. At higher values of magnetic field, the voltage increases with increasing field. The source of this behavior is a switch in the discharge structure from a generally diffusive to a more constricted mode and the Hall effect. The experimental data shows that in general the voltage requirement of the discharge increases as the magnitude of the magnetic field increases beyond 0.3 T for both polarities. Therefore, plasma generation in the presence of a strong magnetic field generally requires higher power supply.

Electrodes parallel to the leading edge of the control surface generate a conductive current vector mostly aligned with the airflow

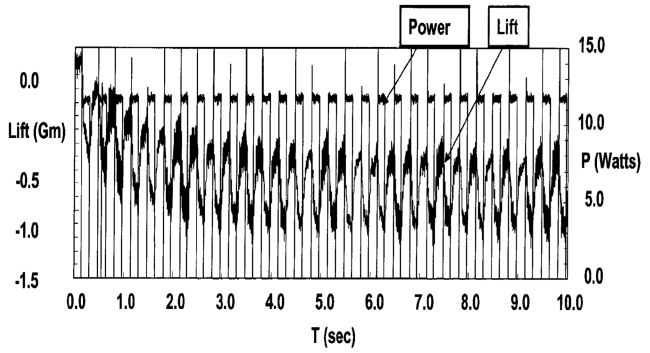

Fig. 11 Rapid and repeatable lift generation by pulsed dc discharge $M_\infty = 5.15$, EMF = 500 V, $I = 24$ mA at 3.0 Hz.

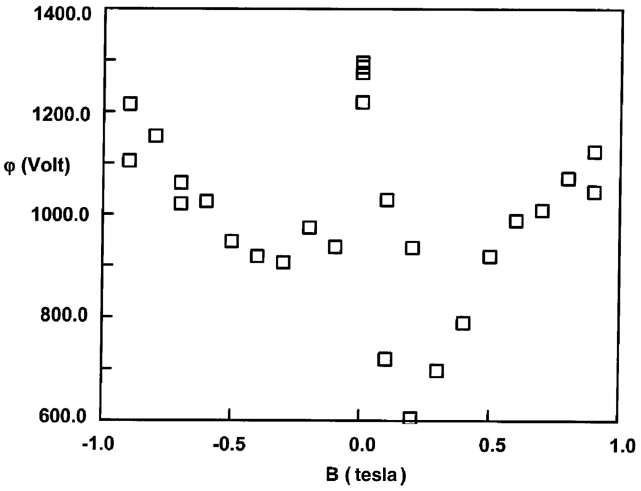

Fig. 12 Hypersonic dc discharge characteristic in transverse magnetic field $I = 50$ mA, $P_\infty = 0.6$ Torr, $U_\infty = 676$ m/s.

[32–34]. In the investigation, a transverse magnetic field is applied across the plasma channel perpendicular to the electric current. By this arrangement, the transverse magnetic field generates a Lorentz force $J \cdot B$ that either expels from ($J \cdot B > 0$) or attracts ($J \cdot B < 0$) the negatively charged particles to the plate surface. It is anticipated for the case in which the charged particles are expelled from the plate surface that the momentum exchange between ions and neutral particles by inelastic collisions will be further enhanced, and the subsequent viscous–inviscid interaction will lead to a greater pressure plateau over the electrodes. Conversely, the restrained discharge particle motion suppresses the intensity of the magneto-aerodynamic interaction. Preliminary experimental observations have confirmed this finding, but uncertainty is evident over a wide range of magnetic field strengths [32–34]. In essence, this net result of magnetoaerodynamic interaction reflects compensating effects between the constricted surface discharge and acceleration by the Lorentz force. The surface plasma already operates in the abnormal discharge regime; the externally applied magnetic field creates additional discharge instability that obscures experimental observation [32–34].

According to the testing condition, the electron Larmor frequency at $B = 1.0$ tesla is 1.76×10^{11} rad/s, and the electron-heavy particle collision frequency is estimated to be in a range from 3.9×10^{9}/s to 2.3×10^{10}/s [29,30]. Under these conditions, the behavior of the plasma in the hypersonic MHD channel is not collisionally dominant, and the maximum and effective Hall parameters range approximately from 7.6 to 45.1. To alleviate the uncertainty, the simulations are limited to a lower magnetic field intensity $-0.2\ \text{T} < B < 0.2\ \text{T}$. The polarity of the field is reversed to generate two possible Lorentz force orientations directed away ($J \cdot B > 0.0$) and toward ($J \cdot B < 0.0$) the plate surface. In Fig. 13, the computed results at a uniform magnetic field but different field polarity are compared with the experimental data. The computed result for $J \cdot B > 0.0$ generally overpredicts the pressure measurement, and the data also exhibit an unusually large data scatter due to the unstable glow discharge in a uniformly applied magnetic field [32–34]. The disparity between data and computational results is more pronounced for the Lorentz force that suppresses the outward motion of charged particles $J \cdot B < 0$ [29]. Meanwhile, an increased effort is also required to maintain computational stability in the presence of an applied magnetic field. The numerical simulation at $B = -0.2$ tesla indicates a diminished induced surface pressure caused by suppressing an outward deflection of the streamlines. However, the numerical result underpredicts the measurements. Nevertheless, the numerical results using the drift-diffusion model capture the difference between the applied magnetic fields of opposite polarity [29,30].

In essence, the hypersonic magneto-fluid-dynamic interaction demonstrates a greater dynamic range for effective flow control and can be adopted as an effective flow control mechanism. However, the plasma generation process, a direct current glow discharge, restricts the effective application range to only a low ambient pressure environment. In addition, the externally applied magnetic field also imposes a vast range of challenges both for the experimental and computational investigation. There are many open issues that must wait for future investigation, but the magneto-fluid-dynamic interaction has shown potential to be a viable hypersonic flow control mechanism.

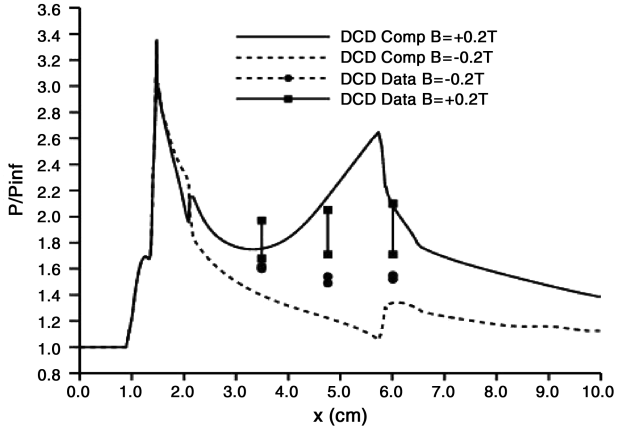

Fig. 13 Induced surface pressure distribution in transverse magnetic field $M_\infty = 5.15$, EMF = 1.2 kV, $I = 50$ mA, $B = \pm 0.2$ T, $P_0 = 370$ torr, $T_0 = 300$ k.

Virtual Variable Geometry Cowl

The approach of using magneto-fluid-dynamic interaction for hypersonic flow control has been fully demonstrated near the leading edge of a control surface. This idea is equally applicable near the leading edge of a rectangular inlet as an MFD compressor [35]. In a side-by-side experimental and computational investigation, a dc discharge is again adopted as the plasma actuator. The electrodes of the dc discharge are embedded in the sidewalls of a constant cross-sectional area inlet; this arrangement is nonintrusive when deactivated. Once the discharge is actuated, the increased slope of the displacement thickness through MFD interaction consistently generates an oblique shock like the side compression of a convergent inlet cowl. The compression is controlled by the plasma generation power input. The induced compression near the leading edge of the inlet emulates a variable geometry cowl.

Figure 14 presents the photograph of an activated dc discharge within a rectangular, constant area inlet. The inlet model is limited to a relatively small dimension of $10.16 \times 3.81 \times 3.11$ cm ($x \times y \times z$) [35]. The four side walls of the model have sharp leading edges with an outward bevel angle of 20 deg. The copper cathode and anode are embedded in opposite Phenolic sidewalls parallel to the z coordinate. Direct current discharge is sustained by the electric potential of 800 V for electrical currents of 80 mA. All electrodes have identical dimensions of $3.175 \times 0.64 \times 0.16$ cm, (length × width × depth). The cathodes are placed a distance of 0.79 cm downstream from the leading edge of the inlet, and the distance between the centerline of the cathode and anode is 2.22 cm. The electric current density on the anode has a value of 21.27 mA/cm^2 under the applied electric potential of 800 V.

The experimental data of the rather small inlet model is restricted to Pitot-pressure data and optical observation. However, the performance of an inlet is measured by the static and stagnation pressure recovery. Therefore, computational simulation becomes pivotal to analyze the critical performance information that is not obtained from experimental measurement. To achieve this goal, a substantial amount of effort has focused on the validation of the physical phenomenon and calibration of the magnitude of the difference between flowfields with and without the activated dc discharge [35].

A typical simulated ion number density close to the experimental condition is depicted in Fig. 15. To highlight only the concentrated discharge domain, only 40 constant-value density contours from 10^7/cm^3 to the maximum of 10^{12}/cm^3 are plotted. The globally neutral plasma with a charged particle concentration less than 10^8/cm^3 is conveyed toward downstream and further diluted by diffusion and recombination. At the local static pressure of 2.5 torr and electric potential of 1000 V, the highest charged particle concentration is located at the outer edge of the plasma sheath

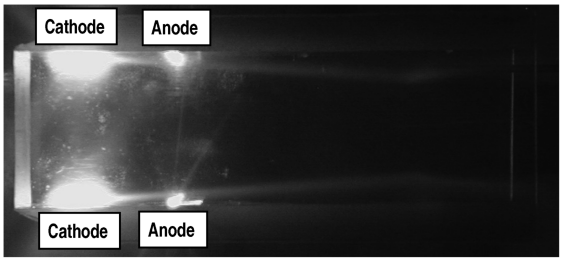

Fig. 14 dc discharge along rectangular inlet sidewalls $M_\infty = 5.15$, EMF = 800 V, $I = 50$ mA, $P_0 = 370$ torr, $T_0 = 300$ k.

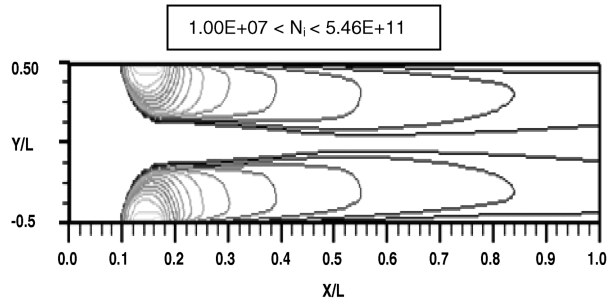

Fig. 15 Computed ion number density of glow discharge in rectangular inlet $M_\infty = 5.15$, EMF = 800 V, $I = 50$ mA, $P_0 = 370$ torr, $T_0 = 300$ k.

(around 5 mm). The dc discharge is operated at the unstable range, and the data exhibit perceptible fluctuations, but the numerical simulations remain steady. Nevertheless, the magnitude of charged particles density agrees with detailed measurements at the similar test condition [35], and the overall structure of the dc discharge pattern bears close resemblance to the experimental observation.

From both the experimental observation and computational simulation, the MFD interaction does not alter the basic flowfield structure within the rectangular inlet. The four sharp and mutually perpendicular leading edges induce four oblique shocks over the side walls. Upstream of the first shock wave intersection, a total of eight triple points of the shock structure are formed [35]. Downstream of the shock wave intersections, the flowfield is characterized by reflected shock waves from the sidewalls and multiple shock-on-shock interactions. The Pitot-pressure distributions along the centerline of the inlet with and without the activated dc discharge on the vertical walls are given in Fig. 16. The oblique shocks strengthened by the dc discharges over the vertical sidewalls have steepened oblique shock angles (16.9 versus 18.0 deg). As a consequence, the shock interaction moves upstream and shows a greater compression ratio. Downstream of the intersection, the flowfield generated by the dc discharge has a slightly lower Mach number and reveals a lower Pitot pressure than the flow with deactivated dc discharge. The computational simulations agree with data both in locations of the shock intersections and the relative magnitude of the Pitot pressures. The MFD interaction generates an 8.6% greater peak Pitot pressure at the shock intersection than the deactivated counterpart.

The computed static pressure distributions along the centerline and on the horizontal sidewall of the inlet are given in Fig. 17. When the dc discharge is activated, the static pressure distribution along the centerline of the inlet is elevated over the unperturbed flow and exhibits the classic pressure plateau upstream of the peak pressure for a shock impingement [45]. On the other hand, the activated dc discharge alters the surface pressure at the leading edge of the inlet

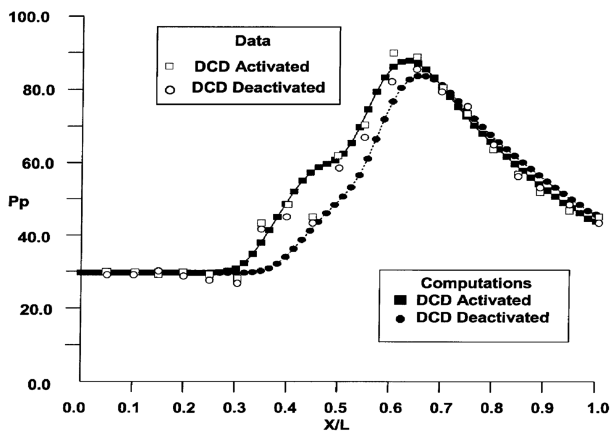

Fig. 16 Validated Pitot pressure along centerline of inlet $M_\infty = 5.15$, EMF = 800 V, $I = 50$ mA, $P_0 = 370$ torr, $T_0 = 300$ k.

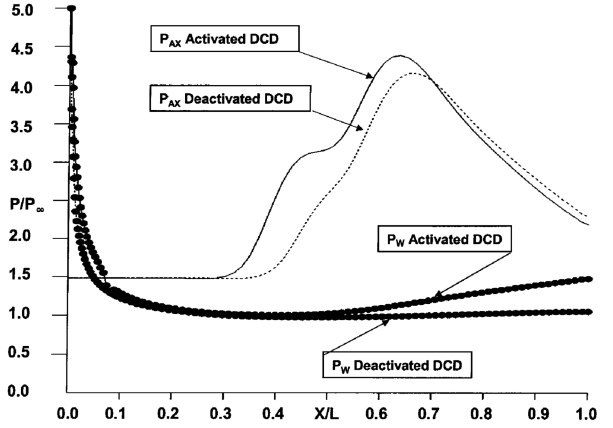

Fig. 17 Computed inlet streamwise static pressure distributions $M_\infty = 5.15$, EMF = 800 V, $I = 50$ mA, $P_0 = 370$ torr, $T_0 = 300$ k.

and a sharp drop in pressure is also observed near the trailing edge of the cathode. However, the most remarkable effect of the sidewall dc discharge is the continuous compression in the near wall regions over all sidewalls. Meanwhile, the unperturbed flow within the inlet has reached a decreasing asymptote of 1.13 torr. The sidewall dc discharge induces a pressure rise to 1.47 torr, a 30% increase at a plasma generation power of 64 W.

Extensive Pitot pressure surveys have been conducted for the MFD interaction within the inlet. The streamwise pressure distributions along the entire length of the inlet at different distances from the sidewall are recorded together with Pitot-pressure profiles at the shock intersection and inlet exit. For the present effort, only the Pitot-pressure distributions near the exit of the inlet ($X/L = 0.95$) are depicted in Fig. 18. Two distributions across the centerline ($Z/L = 0.0$) and near the horizontal wall ($Z/L = 0.80$) are compared with computational results. The overall agreement between data and computed result is reasonable, particularly in view of the fact that the dc discharge is operated in the unstable mode, and the Pitot data has a scattering band as high as 6%. In all, the simulated results capture the multiple shock-on-shock interactions. The maximum discrepancy between time-averaged measurement and computed simulation is determined to be less than 4.6%.

The computed static pressure distribution across the vertical sidewalls and near the inlet exit is presented in Fig. 19. The static pressure distributions represent the crossflow behavior along the central plane of the inlet. When the dc discharge is activated, the steepened oblique shocks parallel to the electrode embedded sidewall intersect upstream of the unperturbed flow counterpart. The shock wave structure with the dc discharge therefore shifts toward inlet centerline in contrast to the unperturbed flow and with a greater

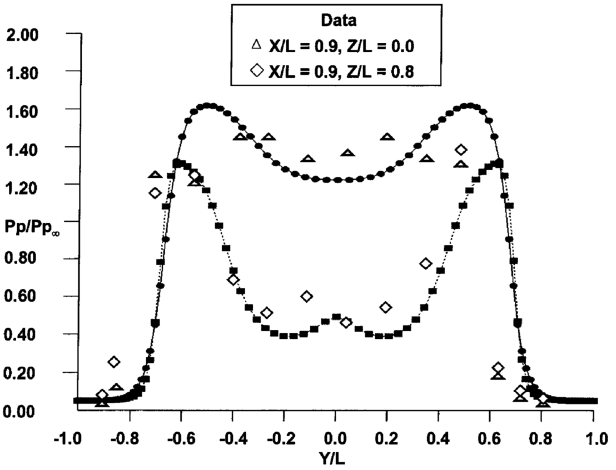

Fig. 18 Validated Pitot-pressure distributions at inlet exit $M_\infty = 5.15$, EMF = 800 V, $I = 50$ mA, $P_0 = 370$ torr, $T_0 = 300$ k.

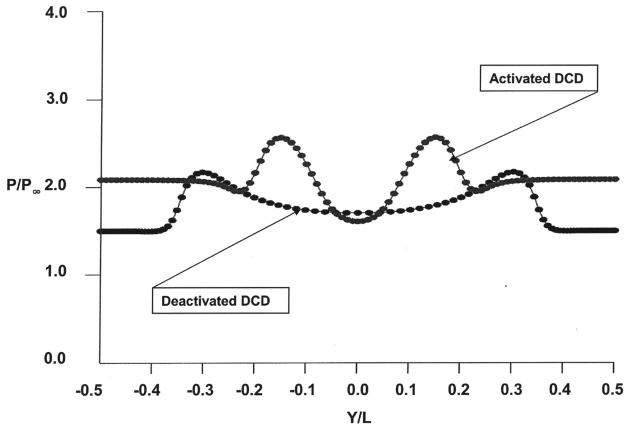

Fig. 19 Computed cross-flow static pressure distributions at inlet exit $M_\infty = 5.15$, EMF = 800 V, $I = 50$ mA, $P_0 = 370$ torr, $T_0 = 300$ k.

shock intensity. The crossflow field also reveals the typical behavior of a viscous–inviscid interaction in that the static pressure is elevated within the boundary layer. This behavior is also detected in the pressure distribution across the horizontal sidewalls [35]. From this figure, the lower static pressure before shock compression by the reflected shock waves is also detected near the centerline of the inlet, as it has been observed from the Pitot-pressure distribution in Fig. 16.

In short, the additional compression induced by the dc discharge at the inlet exit is determined to be 11.6% by integrating the static pressure over the exit plane. This performance of a pair of dc discharges at the entrance of a constant area rectangular inlet emulates a variable geometrical cowl with a deflection angle of 1.2 deg at an entrance Mach number of 5.15. The power requirement for the MFD compression is nearly identical to that observed earlier for the virtual leading edge strake.

Conclusions

The plasma actuator using electromagnetic perturbation of the boundary-layer structure and amplification of the viscous–inviscid interaction for hypersonic flow control has been fully substantiated by experimental observations and numerical simulations with plasma models. The magneto-fluid-dynamic interaction by a plasma actuator embedded in a fixed and nonmovable plate surface behaves like a virtual movable leading-edge strake. For a simple glow discharge over a wedge model at Mach number 5.15, the equivalent deflection angle of the control surface can be as high as 7 deg at a plasma power input of 350 W. Both experimental and computational results have shown the effectiveness of this flow control to be as low as 18 W/cm/ deg of flow deflection. According to the hypersonic pressure interaction theory, the control effectiveness increases with increased Mach number if the electromagnetic perturbation can be sustained.

The basic mechanism of the MFD interaction is determined to be the combined effects of the conductive electrode and volumetric Joule heating. The time scale of Joule heating is estimated in the microsecond range, 3 orders of magnitude shorter than the combined effect of conductive and convective heating in the millisecond regime.

The magnetoaerodynamic interaction exhibits even a greater amplification with an applied external magnetic field than the electroaerodynamic interaction. The drift-diffusion plasma model has been successfully applied to numerical simulations, and the Hall effect is explicitly included in the formulation. In both experiments and computations, the Hall effect significantly constricts the mobility of charged particles and alters the surface discharge pattern. However, the resultant discharge instability obscures both the measurement and computational accuracy.

The MFD interaction is effectively applied to a constant cross-sectional rectangular inlet in hypersonic stream as a virtual variable geometry cowl. The side compression that was traditionally produced by compression ramps is now replaced by the combined effects of a dc discharge and pressure interaction. The computational results indicate a compression of 11.6% over the case with the deactivated dc discharge. The virtual variable geometry cowl is produced by both experimental and computational simulations with a small direct current surface discharge at the entrance region of the inlet.

Acknowledgments

The sponsorship of J. Schmisseur and F. Fahroo of the Air Force Office of Scientific Research is deeply appreciated. The authors are in debt to James Hayes for his invaluable contributions to all aspects of experimental observations and operations of the plasma channel of the Air Vehicle Directorate, Air Force Research Laboratory.

References

[1] Bletzinger, P., Ganguly, B. N., VanWie, D., and Garscadden, A., "Plasma in High Speed Aerodynamics, Topic Review," *Journal of Physics D: Applied Physics*, Vol. 38, No. 4, 2005, pp. R33–57. doi:10.1088/0022-3727/38/4/R01

[2] Fomin, V., Tretyakov, P., Taran, J.-P., "Flow Control Using Various Plasma and Aerodynamic Approaches," *Aerospace Science and Technology*, Vol. 8, No. 5, 2004, pp. 411–421. doi:10.1016/j.ast.2004.01.005

[3] Raizer, Yu. P., *Gas Discharge Physics*, Springer–Verlag, Berlin, 1991.

[4] Howatson, A. M., *An Introduction to Gas Discharges*, 2nd ed., Pergamon Press, Oxford, England, U.K., 1975.

[5] Roth, J. R., Sherman, D. M., and Wilkinson, S. P., "Electrohydrodynamic Flow Control with a Glow-Discharge Surface Plasma," *AIAA Journal*, Vol. 38, No. 7, July 2000, pp. 1166–1172.

[6] Artana, G., D'Adamo, J., Léger, L., Moreau, E., and Touchard, G., "Flow Control with Electrohydrodynamic Actuators," *AIAA Journal*, Vol. 40, No. 9, Sept. 2002, pp. 1773–1779.

[7] Enloe, C. L., McLaughlin, T. E., Vandyken, R. D., and Kachner, K. D., Jumper, E. J., Corke, T. C., Post, M., and Haddad, O., "Mechanisms and Responses of a Single Dielectric Barrier Plasma Actuator: Geometric Effects," *AIAA Journal*, Vol. 42, No. 3, March 2004, pp. 595–604. doi:10.2514/1.3884

[8] Post, M. L., and Corke, T. C., "Separation Control on High Angle of Attack Airfoil Using Plasma Actuator," *AIAA Journal*, Vol. 42, No. 11, 2004, pp. 2177–2184. doi:10.2514/1.2929

[9] Boeuf, J. P., and Pitchford, L. C., "Electrodrodynamic Force and Aerodynamic Flow Acceleration in Surface Dielectric Barrier Discharge," *Journal of Applied Physics*, Vol. 97, No. 103307, May 2005, pp. 103307-1–103307-10.

[10] Shang, J. S., "Solving Schemes for Computational Magneto-Fluid-Dynamics," *Journal of Scientific Computing*, Vol. 25, No. 1, Oct. 2005, pp. 289–306. doi:10.1007/s10915-004-4645-3

[11] Gaitonde, D. V., Visbal, M. R., and Roy, S., "Simulations on Control of Flow Past a Wing Section with DBDs," AIAA Paper 2005-5302, June 2005.

[12] Shang, J. S., and Chang, C. L., "Magneto-Aerodynamic Interaction over Airfoil," AIAA Paper 2005-5179, June 2005.

[13] Visbal, M. R., and Gaitonde, D. V., "Control of Vortical Flows Using Simulated Plasma Actuators," AIAA Paper 2006-0505, 2006.

[14] Fraishtadt, V. L., Kuranov, A. L., and Sheikin, E. G., "Use of MHD Systems in Hypersonic Aircraft," *Technical Physics*, Vol. 43, No. 11, 1998, p. 1309. doi:10.1134/1.1259189

[15] Park, C., Mehta, U. B., and Bogdanoff, D. W., "MHD Energy Bypass Scramjet Performance with Real Gas Effects," *Journal of Propulsion and Power*, Vol. 19, No. 5, 2001, pp. 1049–1057.

[16] Gaitonde, D. V., "Three-Dimensional Flow-Through Scramjet Simulation with MGD Energy-Bypass," AIAA Paper 2003-0172, Jan. 2003.

[17] Bityurin, V., Klimov, A., and Leonov, S., "Assessment of a Concept of Advanced Flow/Flight Control for Hypersonic Flights in Atmosphere," AIAA Paper 99-4820, Nov. 1999.

[18] Leonov, S., Bityurin, V., Savelkin, K., and Yarantsev, D., "Effect of Electrical Discharge on Separation Processes and Shock Position in Supersonic Airflow," AIAA Paper 2002-0355, Jan. 2002.

[19] Resler, E. L., and Sears, W. R., "The Prospect for Magneto-Aerodynamics," *Journal of Aerospace Science*, Vol. 25, 1958, pp. 235–245, 258.

[20] Ganiev, Y., Gordeev, V., Krasilnikov, A., Lagutin, V., Otmennikov, V., and Panasenko, "Aerodynamic Drag Reduction by Plasma and Hot-Gas Injection," *Journal of Thermophysics and Heat Transfer*, Vol. 14, No. 1, 2000, pp. 10–17.
[21] Shang, J. S., "Plasma Injection for Hypersonic Blunt Body Drag Reduction," *AIAA Journal*, Vol. 40, No. 10, 2002, pp. 1178–1186.
[22] Shang, J. S., Hayes, J. R., and Menart, J., "Hypersonic Flow over a Blunt Body with Plasma Injection," *Journal of Spacecraft and Rockets*, Vol. 39, No. 3, 2002, pp. 367–375.
[23] Adelgren, R. G., Yan, H., Elliott, G. S., Knight, D. D., Beutner, T. J., and Zheltovodov, A. A., "Control of Edney IV Interaction by Pulsed Laser Energy Deposition," *AIAA Journal*, Vol. 43, No. 2, Feb. 2005, pp. 256–269. doi:10.2514/1.7036
[24] Kandala, R., and Candler, G. V., "Numerical Studies of Laser-Induced Energy Deposition for Supersonic Flow Control," *AIAA Journal*, Vol. 42, No. 11, 2004, pp. 2266–2275. doi:10.2514/1.6817
[25] Macheret, S. O., Shneider, M. N., and Miles, R. B., "Magneto-hydrodynamic Control of Hypersonic Flows and Scramjet Inlets Using Electron Beam Ionization," *AIAA Journal*, Vol. 40, No. 1, Jan. 2002, pp. 74–81.
[26] Macheret, S. O., Shneider, M. N., and Miles, R. B., "Scramjet Inlet Control by Off-Body Energy Addition: A Virtual Cowl," *AIAA Journal*, Vol. 42, No. 11, 2004, pp. 2294–2302. doi:10.2514/1.3997
[27] Kolesnichenko, Y., "Basics in Beams MW Energy Deposition for Flow/Flight Control," AIAA Paper 2004-0669, Jan. 2004.
[28] Macheret, S. O., Shneider, M. N., and Miles, R. B., "Magneto-hydrodynamics and Electro-hydrodynamic Control of Hypersonic Flows of Weakly ionized Plasmas," *AIAA Journal*, Vol. 42, No. 7, July 2004, pp. 1378–1387. doi:10.2514/1.3971
[29] Shang, J. S., and Surzhikov, S. T., "Magneto-Aerodynamic Actuator for Hypersonic Flow Control," *AIAA Journal*, Vol. 43, No. 8, 2005, pp. 1633–1643. doi:10.2514/1.6625
[30] Shang, J. S., Surzhikov, S. T., Kimmel, R. L., Gaitonde, D. V., Menart, J. A., and Hayes, J. R., "Mechanisms of Plasma Actuator for Hypersonic Flow Control," *Progress in Aerospace Sciences*, Vol. 41, No. 8, 2005, pp. 642–668. doi:10.1016/j.paerosci.2005.11.001
[31] Menart, J., Shang, J., Henderson, S., Kurpik, A., Kimmel, R., and Hayes, J., "Survey of Plasma Generated in a Mach 5 Wind Tunnel," AIAA Paper 2003-1194, Jan. 2003.
[32] Menart, J., Shang, J. S., Kimmel, R., and Hayes, J., "Effects of Magnetic Fields on Plasma Generated in Mach 5 Wind Tunnel," AIAA Paper 2003-4165, June 2003.
[33] Kimmel, R., Hayes, J., Menart, J., and Shang, J. S., "Effect of Surface Plasma Discharges on Boundary Layer at Mach 5," AIAA Paper 2004-0509, Jan. 2004.
[34] Kimmel, R., Hayes, J., Menart, J., and Shang, J. S., "Effect of Magnetic Fields on Surface Plasma Discharges at Mach 5," *Journal of Spacecraft and Rockets*, Vol. 43, No. 6, 2006, pp. 1340–1346. doi:10.2514/1.14247
[35] Shang, J. S., Menart, J., Kimmel, R., and Hayes, J., "Hypersonic Inlet with Plasma Induced Compression," AIAA Paper 2006-0764, 2006.
[36] Leonov, S. B., Yarantsev, D. A., Gromov, V. G., and Kuriachy, A. P., "Mechanisms of Flow Control by Near-Surface Electrical Discharge Generation," AIAA Paper 2005-0780, Jan. 2005.
[37] Sutton, G. W., and Sherman, A., *Engineering Magnetohydrodynamics*, McGraw–Hill, New York, 1965, pp. 295–339.
[38] Mitchner, M., and Kruger, C. H., *Partially Ionized Gas*, Wiley, New York, 1973.
[39] Hayes, W. D., and Probstein, R. F., *Hypersonic Flow theory*, Academy Press, New York, 1959, pp. 333–374.
[40] Surzhikov, S. T., and Shang, J. S., "Two-Component Plasma Model for Two-dimensional Glow Discharge in Magnetic Field," *Journal of Computational Physics*, Vol. 199, No. 2, 2004, pp. 437–464. doi:10.1016/j.jcp.2004.02.019
[41] Surzhikov, S. T., and Shang, J. S., "The Hypersonic Quasineutral Gas Discharge Plasma in a Magnetic Filed," MIT Paper 230-330, 2005.
[42] Shang, J. S., Kimmel, R., Hayes, J., Tyler, C., and Menart, J., "Hypersonic Experimental Facility for Magnetoaerodynamic Interaction," *Journal of Spacecraft and Rockets*, Vol. 42, No. 5, 2005, pp. 780–789. doi:10.2514/1.8579
[43] Cabannes, H., *Theoretical Magnetofluiddynamics, Applied Mathematics and Mechanics*, Academic Press, New York, 1970, p. 11.
[44] Menart, J., Stanfield, S., Shang, J. S., Kimmel, R., and Hayes, J., "Study of Plasma Electrode Arrangements for Optimum Lift in a Mach 5 Flow," AIAA Paper 2006-1172, Jan. 2006.
[45] Shang, J. S., Hankey, W. L., and law, C. H., "Numerical Simulation of Shock Wave-Turbulent Boundary Layer Interaction," *AIAA Journal*, Vol. 14, No. 10, Oct. 1976, pp. 1451–1457.

S. Macheret
Guest Editor